Chinese Chemical Letters 32 (2021) 870–874

Contents lists available at ScienceDirect

Chinese Chemical Letters

journal homepage: www.elsevier.com/locate/cclet

Communication

Dependence of electromagnetic wave absorption properties on the topography of Ni anchoring on reduced graphene oxide

Luyang Liang[a,1], Zhaoyang Li[a,1], Zhongyi Bai[b], Yuezhan Feng[a,*], Xiaoqin Guo[b,*], Jianmin Ma[c,*], Chuntai Liu[a]

[a] Key Laboratory of Advanced Materials Processing & Mold, Ministry of Education, National Engineering Research Center for Advanced Polymer Processing Technology, Zhengzhou University, Zhengzhou 450002, China
[b] Henan Key Laboratory of Aeronautical Materials and Application Technology, School of Material Science and Engineering, Zhengzhou University of Aeronautics, Zhengzhou 450046, China
[c] Key Laboratory for Micro-/Nano-Optoelectronic Devices, Ministry of Education, School of Physics and Electronics, Hunan University, Changsha 410022, China

ARTICLE INFO

Article history:
Received 18 May 2020
Received in revised form 6 June 2020
Accepted 9 June 2020
Available online 9 June 2020

Keywords:
Ni/rGO
Morphology structure
Magnetic coupling effect
Synergistic effect
Electromagnetic wave absorption

ABSTRACT

Specific topographic Ni anchoring on reduced graphene oxide (rGO) composites show an astronomical potential as effective wave absorbers due to the synergistic electromagnetic loss effects. Herein, Ni/rGO composites with different topography were successfully prepared *via* hydrothermal *in-situ* reduction method. The structure and morphology characteristics revealed that particle-like, chain-like, coin-like and flower-like Ni were closely anchored onto rGO, respectively. The electromagnetic wave absorption (EMA) performance revealed that chain-like Ni/rGO exhibited the optimal reflection loss of -43.7 dB with a thickness of 1.8 mm as well as the EAB of 6.1 GHz at 2.0 mm among all samples due to the good impedance match and the synergistic dielectric and magnetic losses. Besides, one conclusion can be drawn that excellent magnetic coupling effect and impedance matching were the main reasons for significantly improving the EMA performance. Considering the systematic dependence of morphology on EMA, this work provides a perspective for designing high-performance absorbing materials.

With the rapid proliferation of advanced electronic devices and precision radar networks working in the gigahertz (GHz) band, the growing electromagnetic (EM) interference often causes serious harm to the environment and human health [1,2]. As a consequence, designing and developing of lightweight and high-efficiency electromagnetic absorbing (EMA) materials has become a huge challenge for researchers to deal with the EM wave pollution and the aircraft stealth problems [3,4].

Traditionally, magnetic metals, such as Fe, Co, Ni, have been widely used as EMA materials due to their desired conductive and magnetic loss for EM waves [5]. However, unilateral magnetic metals with large density cannot meet the requirements of light-weight, small volume and corrosion resistance at the same time in practical applications [6]. Therefore, combining magnetic metals and dielectric materials has been developed as an effective strategy for preparing high-efficient and practical EMA materials. For example, Xiao *et al*. obtained a lightweight magnetic hybrid composed of Co and carbon nanotubes (CNTs), and the optimal absorption effect of -49.16 dB at 2.5 mm can be detected [7]. Recently, especially since many 2D lightweight dielectric materials including graphene [8], MXene [9] and MoS_2 [10] have been discovered and applied, hybrids of magnetic metals and 2D materials have gradually become one of designing hotspots in EMA field. Among them, reduced graphene oxide (rGO) not only exhibits a high specific surface area and excellent electrical conductivity, but also remains large number of oxygen-containing functional groups for dipole polarization, which make rGO-based composites be very promising for applications in EM wave absorbing and shielding [11–14]. For instance, Zhao *et al*. reported an ultra-thin CoNi/rGO aerogel with a $RL_{\min}$ value of -53.3 dB and an effective bandwidth of 3.5 GHz at only 0.8 mm [15]. From above, one can be noticed that the hybridization of rGO and magnetic metals plays a crucial role in promoting the EM wave absorption. In addition to the inherent characteristics of materials, the micro-morphology of magnetic metals also has a crucial effect on the absorption of EM waves [16,17]. There have been some reports showing different EMA effects of individual topography of Ni/rGO (*e.g.*, urchin [18], flower

---

[*] Corresponding authors.
E-mail addresses: yzfeng@zzu.edu.cn (Y. Feng), guoxq@zua.edu.cn (X. Guo), nanoelechem@hnu.edu.cn (J. Ma).

[1] These authors contributed equally to this work.

https://doi.org/10.1016/j.cclet.2020.06.014
1001-8417/

[19], particle-like [20]). Unfortunately, as far as we know, there are rare reports on exploring the topography dependence of Ni on EMA property of its rGO hybrid under the same standard.

In this work, Ni/rGO with different topographical nano-Ni were fabricated *via* unified hydrothermal *in-situ* reduction technology by changing additives and reaction conditions (see Experimental section and Table S1 in Supporting information for details). Taking the formation process of chain-like Ni/rGO as an example, the forming mechanism has been studied deeply, which is shown in Fig. S1 (Supporting information). The result revealed that chain-like nano-Ni loaded on rGO was able to exert the more absorbing potential of hybrids comparing to others with particle-like, coin-like and flower-like topography nano-Ni. More importantly, the absorbing mechanism in chain-like Ni/rGO hybrids was proposed based on EM loss theory, which may provide a reference for the design of the EMA material's perimeter structure.

On the basis of the transmission line theory, the reflection loss value of EMA material can be evaluated by the following equations (Eqs. 1 and 2) [21]:

$$RL = 20\log_{10}|(Z_{in} - Z_0)/(Z_{in} + Z_0)| \tag{1}$$

$$Z_{in} = Z_0\sqrt{\frac{\mu_r}{\varepsilon_r}}\tanh\left(j\frac{2\pi f d\sqrt{\mu_r\varepsilon_r}}{c}\right) \tag{2}$$

where Z_{in} is input impedance, Z_0 is the impedance of free space, f is frequency, d is thickness and c is the velocity of light. When reflection loss (RL) < 10 dB, more than 90% of EM wave is absorbed, and the corresponding frequency range is called effective absorption band (EAB).

The morphologies and microstructures of Ni/rGO were characterized by SEM (Fig. 1). Fig. 1a reveals the particle-like Ni with size of about 200 nm is uniformly and regularly anchored on rGO surface. Fig. 1b exhibits that the chain-like Ni was formed by connecting Ni nanoparticles each other with an average diameter of 0.8 μm, which closely adheres on rGO surface. Noteworthily, the unique one dimension (1D) structure showing a large long diameter and strong magnetic anisotropy is conducive to receiving more EM waves [22]. By contrast, coin-like Ni seems to easily cause agglomeration and densification on rGO surface due to mutual in-plane attraction (Fig. 1c), which is adverse for the dispersion and interfacial polarization of the absorbing material. Fig. 1d reveals the flower-like Ni embedding on the surface of rGO. In addition, rGO in all samples exhibits a crepe-like transparent gauze structure. The appearance of wrinkles is mainly due to the reduction of the carbon skeleton integrity and the residual of oxygen-containing functional groups during the reduction of GO, which is beneficial to increase the transmission path and space of EM waves and dipole polarization [23].

Fig. 1e shows the XRD patterns of the prepared samples. It can be seen that the all samples reveal the typical diffraction peaks at $2\theta = 44.51°$, $51.85°$ and $76.37°$ corresponding to (111), (200) and (220) crystal planes of Ni (Nickel, JCPDF#04–0850), respectively. Clearly, there is no other diffraction peaks appear, indicating that GO and Ni^{2+} have been reduced to rGO and Ni under the action of reductants, and confirming Ni/rGO composites have been prepared successfully. From the Raman spectra of Ni/rGO (Fig. 1f), two main peaks at 1345 cm^{-1} and 1595 cm^{-1} corresponding to the D and G bonds of rGO, respectively, can be observed. The I_D/I_G determining structural defects in different topography of Ni/rGO hybrids are 1.07, 1.09, 1.02 and 1.03, respectively. The largest I_D/I_G value of chain-like Ni/rGO means more structural defects in rGO produced by reduction process, which may be attributed to the weak reducibility of NaH_2PO_2 and $C_4H_4O_6KNa$. It is worth noting that the presence of defects is beneficial to the EMA properties of Ni/rGO hybrids. FT-IR spectra of as prepared Ni/rGO samples (Fig. S2 in Supporting information) also reveal that the oxygen-containing functional groups such as —OH remain after being reduced. These functional groups, as well as the defects at surface or edge, can form the polarization centers during the interaction with EM waves, which would promote the dipole and interfacial polarization effects and thus attenuate more EM waves [24].

EMA properties of absorbing materials are closely related with the relative complex permittivity ($\varepsilon_r = \varepsilon'-j\varepsilon''$), relative complex permeability ($\mu_r = \mu'-j\mu''$) and their loss tangent (dielectric loss tangent: $\tan\delta_\varepsilon = \varepsilon''/\varepsilon'$; magnetic loss tangent: $\tan\delta_\mu = \mu''/\mu'$), where, the real parts (ε', μ') represent the storage of electrical and

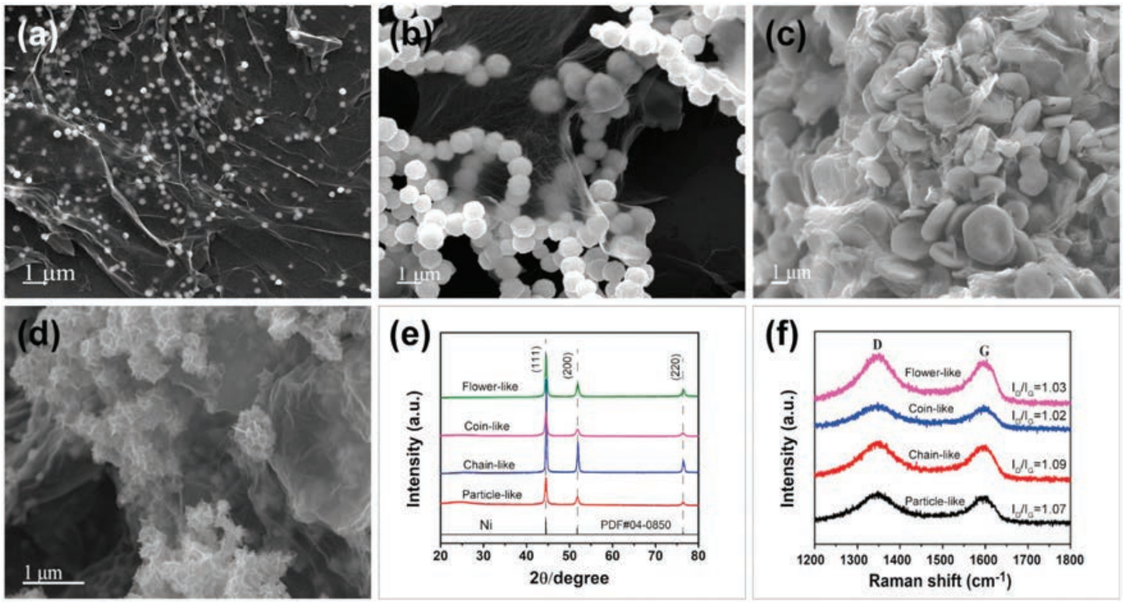

Fig. 1. SEM images of Ni/rGO hybrids with (a) particle-like, (b) chain-like, (c) coin-like and (d) flower-like Ni; (e) XRD and (f) Raman patterns of them.

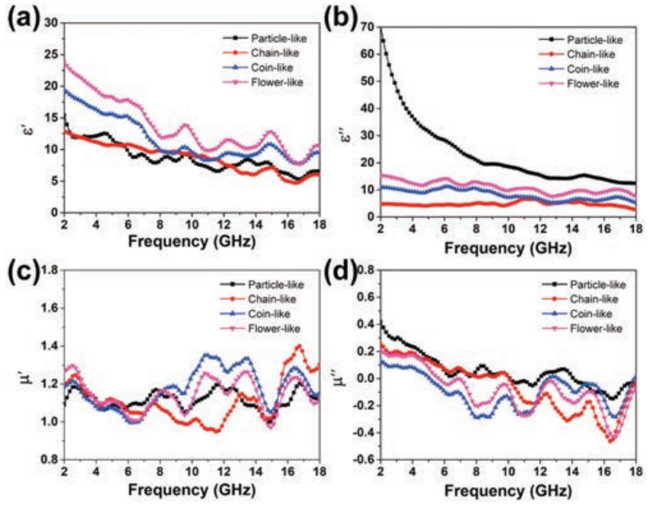

Fig. 2. Frequency dependence of (a) real parts of complex permittivity; (b) imaginary parts of complex permittivity; (c) real parts of complex and (d) imaginary parts of complex permeability for Ni/rGO hybrids.

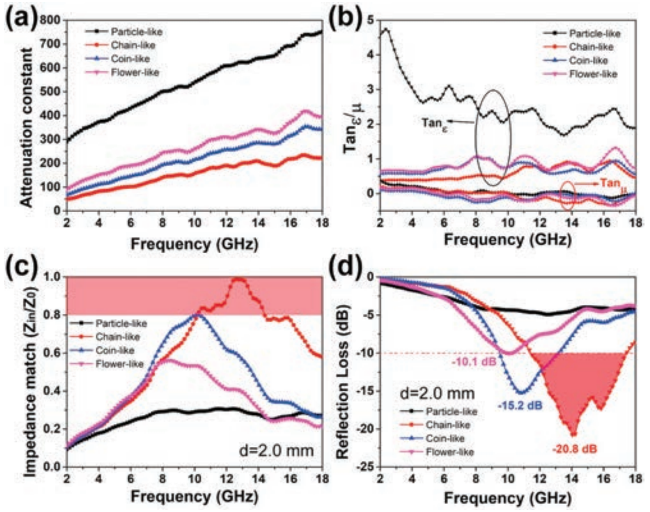

Fig. 3. (a) Attenuation constant; (b) dielectric/magnetic loss tangent; (c) impedance match of Ni/rGO hybrids and (d) corresponding *RL-f* curves at 2.0 mm.

magnetic energy, while the imaginary parts (ε'', μ') represent the loss of electrical and magnetic energy [25]. Figs. 2a and b show the ε' and ε'' of Ni/rGO hybrids in the range of 2−18 GHz. Overall, as the frequency increases, both the ε'-f and ε''-f curves show a slight downward trend. The difference in ε' and ε'' values of the four samples confirms that different morphologies of Ni have a significant effect on the dielectric constant and loss. It can be found that particle-like Ni/rGO reveals the smallest ε′ but largest ε″. This is possible because the fact that the size of Ni particles is smaller than that of other topographies of nano-Ni, which has less effect on the electron conduction between rGO sheets in paraffin matrix. According to the free electron theory ($\varepsilon'' \approx 1/2\pi\varepsilon_0\rho f$, where ρ is resistivity), a higher ε'' means the higher conductivity of particle-like Ni/rGO, which in turn not favors the incidence of EM waves [26]. Comparing with other three different Ni/rGO hybrids, chain-like Ni/rGO hybrid has a both small ε'' and ε', which may be caused by the fact that Ni nanochains link each other to form a network space structure, making themselves unable to contact graphene more completely, thus forming less interface polarization during EM radiation. In addition, multiple fluctuation peaks can be observed in all Ni/rGO hybrids since the nonlinear dielectric resonance caused by different polarizations. For permeability, the μ' value of all samples fluctuates around 1.1, while μ'' shows a decreasing trend and exhibits a negative value at high frequency region (Figs. 2c and d). According to Maxwell's equation, the negative μ'' value is because the external magnetic field is canceled by the induced magnetic field generated by the alternating electric field inside Ni/rGO hybrids. Generally, the magnetic loss of magnetic materials can be mainly attributed to natural resonance, exchange resonance and eddy current effects. Herein, the resonance peaks of μ' and μ'' in 4−7 GHz and 14−18 GHz range can be attributed to natural resonance and exchange resonance, respectively. Eddy current can be expressed by $C_0 = \mu''(\mu')^{-2}f^{-1}$, and the stabilization of C_0-f curves means that the magnetic loss is caused by the eddy current, otherwise it is due to natural resonance or exchange resonance [27]. As shown in C_0-f curves (Fig. S3 in Supporting information), it can be confirmed that the magnetic loss of chain-like Ni/rGO hybrid is caused by eddy current between 7−10 GHz. Moreover, adjacent hybrids would act each other, resulting in the interactive expansion of dense magnetic lines of force, even in the non-magnetic space. In an alternating EM field, the existence of the magnetic coupling effect can produce a huge 3D network space between adjacent Ni particles to attenuate the magnetic field of EM waves [28]. However, for dispersed other shapes of Ni on rGO surface, the longer interval between magnetic particles is not conducive to the dense magnetic coupling effect.

As shown in Fig. 3a, attenuation constant α, representing the ability of converting incident EM waves into heat or other energy, can be indicated as:

$$\alpha = \frac{\sqrt{2}\pi f}{c} \times \sqrt{(\mu''\varepsilon'' - \mu'\varepsilon') + \sqrt{(\mu''\varepsilon'' - \mu'\varepsilon')^2 + (\mu'\varepsilon'' + \mu''\varepsilon')^2}} \tag{3}$$

Similar to the trend of ε''-f curve, the results of α reveal that particle-like Ni/rGO shows a strongest EM wave attenuation ability, while chain-like Ni/rGO is weakest one. Besides, $\tan\delta_\varepsilon$ and $\tan\delta_\mu$ representing the ability of electrical and magnetic energy to be attenuated during the process of EM wave attenuation (Fig. 3b) reveal a similar result with α. Moreover, it can be found that $\tan\delta_\varepsilon$ is greater than $\tan\delta_\mu$, which indicates that dielectric loss dominates the attenuation capacity of EM waves. Even so, as we all know, excellent EMA properties require proper impedance matching to make EM waves enter into absorbing materials and then attenuate them. In other words, the primary condition for EM waves to be attenuated is that sufficient EM waves can be incident.

Especially, 1D Ni nanochain with antenna-like structure is considered to be able to form point charge and micro-current at the tip to better accept EM waves. Contrary to attenuation ability, chain-like Ni/rGO hybrid shows the closest tangent values ($\tan\delta_\varepsilon \approx \tan\delta_\mu$), which implies a more suitable impedance matching [29]. From Eq. 2, the values of $|Z_{in}/Z_0|$ representing the impedance matching were calculated and shown in Fig. 3c. It is obtained that in 10−16 GHz, the $|Z_{in}/Z_0|$ value of chain-like Ni/rGO hybrid is closer to 1 comparing to others, meaning that more EM waves can be received. Recently, on the basis of the impedance matching theory, the degree of impedance matching (Δ) can further confirm this explanation, which can be determined as follows (Eqs. 4–6) [30]:

$$|\Delta| = \left|\sinh^2(Kfd) - M\right| \quad (4)$$

$$K = \frac{4\pi\sqrt{\varepsilon'\mu'\sin\frac{\delta_\varepsilon+\delta_\mu}{2}}}{c\cos\delta_\varepsilon\cos\delta_\mu} \quad (5)$$

$$M = \frac{4\mu'\varepsilon'\cos\delta_\varepsilon\cos\delta_\mu}{(\mu'\cos\delta_\varepsilon - \varepsilon'\cos\delta_\mu) + \left[\tan\left(\frac{\delta_\mu}{2} - \frac{\delta_\varepsilon}{2}\right)\right]^2(\mu'\cos\delta_\varepsilon + \varepsilon'\cos\delta_\mu)^2} \quad (6)$$

A smaller $|\Delta|$ value indicates the better impedance matching. As shown in Figs. S4a-d (Supporting information), as the colored area (particularly less than 0.6) of chain-like Ni/rGO is much larger than other samples at different sample thicknesses, indicating that it has best impedance matching degree among all Ni/rGO hybrids. Based on the above discussion, one can be concluded that chain-like Ni/rGO hybrid exhibits the best impedance matching and suitable EM wave attenuation ability, thereby, it is expected to have the optimal EMA performance. On the grounds of the VNA test results, the EMA properties of Ni/rGO hybrids at 2.0 mm thickness are shown in Fig. 3d. The $RL_{\min}$ of different topography Ni/rGO hybrids is -4.7 dB, -20.8 dB, -15.2 dB and -10.1 dB, respectively. By comparison, in consistent with above-mentioned analyses, chain-like Ni/rGO reveals the best EMA performance with a wide EAB of 6.1 dB.

According to Eq. 2, *d* is one of the key parameters of EMA performance. Therefore, in order to better understand the EMA performance, Figs. 4a and b depict the *RL-f* curves and 3D curves of chain-like Ni/rGO at different sample thickness. It can be seen that at 1.8 mm, a double absorption peak occurs at 15.4 and 16.2 GHz with the $RL_{\min}$ of -25.0 and -43.7 dB, respectively. The existence of double absorption peaks is conducive to strong EM wave loss in multiple frequency bands. Besides, at this thickness, the EAB can reach to 4.5 GHz from 13.5 GHz to 18 GHz. Further increasing the thickness to 2.0 mm, the corresponding EAB can be widened to 6.1 GHz. In particular, as the thickness increases, the absorption band gradually moves towards lower frequencies (Fig. S5 in Supporting information), which can be well illustrated by the quarter-wave ($\lambda/4$) cancellation theory [26,31], that is, when incident wave and reflected wave are 180° out of phase, the reflected wave can be completely eliminated at the surface of absorbers, thus resulting in the migration of the absorption band. The 3D *RL-f-d* curves of other samples are also reflected in Fig. S6 (Supporting informaton). In consistent with the analysis results, chain-like Ni/rGO reveals the best EMA effect at different sample thickness. Compared with previous reports (Table S2 in Supporting informaton) [18,29,32–36], our chain-like Ni/rGO hybrid has the advantages in light weight, strong absorbing ability, thin thickness and absorbing frequency bandwidth.

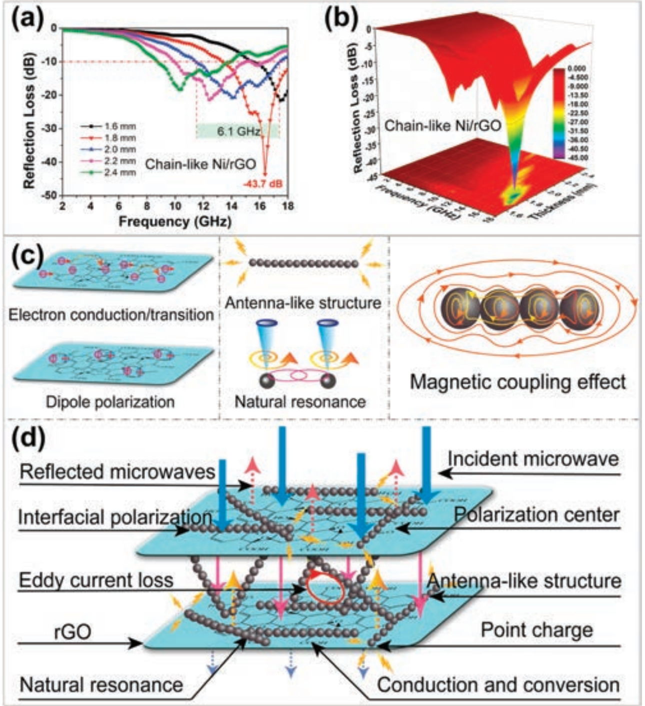

Fig. 4. (a) *RL-f* and (b) 3D *RL-f-d* curves of chain-like Ni/rGO with various thicknesses; (c, d) EMA mechanisms of chain-like Ni/rGO hybrid.

The above results confirm that the anchored nano-Ni on rGO with different morphologies have significant effects on the EMA properties of hybrids. Chain-like Ni/rGO reveals a strong absorption ability due to the good impedance match and the synergistic loss effect between dielectric loss (*e.g.*, conductance loss and polarization relaxation) and magnetic loss (*e.g.*, magnetic resonance and magnetic coupling effects) as shown in Fig. 4c. In order to understand the full EM loss mechanism, the possible interactions between the EM wave and Ni/rGO are summarized in Fig. 4d and Fig. S7 (Supporting information). First of all, when 1D chain/antenna-like Ni interacts with alternating EM field, the electrons accumulate at the tip of Ni chains, which can form a point charge, and then EM energy is converted into a micro-current by means of electronic conduction to be dissipated [37]. Secondly, the chain-like features of Ni/rGO are considered to form a spatial 3D network in the paraffin sample to amplify the magnetic coupling effect and form a stable attenuation effect on the applied EM field. Thirdly, in Ni/rGO hybrid, the large aspect ratio of 1D chain-like Ni and 2D rGO prolongs the EM wave transmission path, which is beneficial to attenuate EM waves. Correspondingly, the thermal energy generated by the EM reaction can be transferred to the thermal conductive rGO on both sides in time, thereby achieving the effect of rapid heat dissipation. Fourth, under the alternating EM field, dipole polarization relaxation and interfacial polarization relaxation caused by the rearrangement of electrons between Ni/rGO, Ni/paraffin, and rGO/paraffin are also considered to be an important dissipation mechanism.

In summary, magnetic nano-Ni with diverse morphologies loading rGO hybrids were synthesized *via* hydrothermal *in-situ* reduction method. Morphology and structure characteristics of Ni/rGO hybrids were cleared through XRD, SEM, FT-IR and Raman tests. In addition, the EM parameters of Ni/rGO samples were tested and discussed between 2–18 GHz. Significantly, results revealed that chain-like Ni/rGO hybrid show an excellent impedance matching and the synergistic loss effect between dielectric loss and magnetic loss, which heavily improves its acceptance and attenuation of EM waves. When the absorber thickness is 1.8 mm, the $RL_{\min}$ can reach -43.7 dB, as well as EAB can come up to 6.1 GHz at 2.0 mm. In short, chain-like Ni/rGO hybrid exhibits the promising characters of wide absorbing waveband, thin thickness and strong EMA performance, which are expected to be applied in military and commercial fields.

Declaration of competing interest

The authors declare that they have no known competing financial interests or personal relationships that could have appeared to influence the work reported in this paper.

Acknowledgments

The authors gratefully acknowledge the financial support for this work by the National Natural Science Foundation of China (Nos. 51903223 and U1704162), China Postdoctoral Science Foundation (No. 2018M642781).

Appendix A. Supplementary data

Supplementary material related to this article can be found, in the online version, at doi:https://doi.org/10.1016/j.cclet.2020.06.014.

References

[1] B. Yao, W. Hong, T. Chen, et al., Adv. Mater. 32 (2020) 1907499.
[2] H. Xu, X. Yin, X. Li, et al., ACS Appl. Mater. Interfaces 11 (2019) 10198–10207.
[3] D. Liu, Y. Du, F. Wang, et al., Carbon 157 (2020) 478–485.
[4] X. Fan, M. Li, X. Li, et al., Chin. Chem. Lett. 31 (2020) 1026–1029.
[5] M. Cao, C. Han, X. Wang, et al., J. Mater. Chem. C 6 (2018) 4586–4602.
[6] J. Tang, N. Liang, L. Wang, et al., Carbon 152 (2019) 575–586.
[7] X. Xiao, W. Zhu, Z. Tan, et al., Compos. B. Eng. 152 (2018) 316–323.
[8] F. Ye, Q. Song, Z. Zhang, et al., Adv. Funct. Mater. 28 (2018) 1707205.
[9] L. Liang, R. Yang, G. Han, et al., ACS Appl. Mater. Interfaces 12 (2020) 2644–2654.
[10] X. Lin, J. Wang, Z. Chu, et al., Chin. Chem. Lett. 31 (2020) 1124–1128.
[11] X. Wang, Y. Lu, T. Zhu, S. Chang, W. Wang, Chem. Eng. J. 388 (2020) 124317.
[12] X. Wang, J. Shu, X. He, et al., ACS Sustain. Chem. Eng. 6 (2018) 14017–14025.
[13] Y. Feng, G. Han, B. Wang, et al., Chem. Eng. J. 379 (2020) 122402.
[14] Y. Feng, B. Wang, X. Li, et al., Carbon 146 (2019) 650–659.
[15] H. Zhao, J. Cheng, J. Zhu, Y. Wang, J. Mater. Chem. C 7 (2019) 441–448.
[16] B. Zhao, W. Zhao, G. Shao, B. Fan, R. Zhang, ACS Appl. Mater. Interfaces 7 (2015) 12951–12960.
[17] H. Wu, J. Liu, H. Liang, D. Zang, Chem. Eng. J. 393 (2020) 124743.
[18] G. Liu, W. Jiang, D. Sun, Y. Wang, F. Li, Appl. Surf. Sci. 314 (2014) 523–529.
[19] L. Wang, H. Xing, S. Gao, X. Ji, Z. Shen, J. Mater. Chem. C 5 (2017) 2005–2014.
[20] K. Xu, W. Ma, Y. Liu, et al., J. Mater. Sci. -Mater. Electron. 30 (2019) 9133–9142.
[21] M. Huang, L. Wang, K. Pei, et al., Small 16 (2020) 2000158.
[22] L. Liang, X. Guo, Z. Bai, B. Zhao, R. Zhang, Powder Technol. 319 (2017) 245–252.
[23] B. Zhao, L. Liang, J. Deng, et al., CrystEngComm 19 (2017) 6579–6587.
[24] S. Wang, Q. Jiao, X. Liu, et al., ACS Sustain. Chem. Eng. 7 (2019) 7004–7013.
[25] S. Gao, G.S. Wang, L. Guo, S.H. Yu, Small 16 (2020) 1906668.
[26] L. Liang, G. Han, Y. Li, et al., ACS Appl. Mater. Interfaces 11 (2019) 25399–25409.
[27] X. Shi, W. You, Y. Zhao, et al., Nanoscale 11 (2019) 17270–17276.
[28] Z. Wu, K. Pei, L. Xing, et al., Adv. Funct. Mater. 29 (2019) 1901448.
[29] J. Feng, F. Pu, Z. Li, et al., Carbon 104 (2016) 214–225.
[30] N. Yang, Z. Luo, S. Chen, G. Wu, Y. Wang, ACS Appl. Mater. Interfaces 12 (2020) 18952–18963.
[31] Z. Jia, D. Lan, K. Lin, et al., J. Mater. Sci. -Mater. Electron. 29 (2018) 17122–17136.
[32] B. Zhao, X. Zhang, J. Deng, et al., PCCP 20 (2018) 28623–28633.
[33] B. Zhao, B. Fan, G. Shao, et al., Appl. Surf. Sci. 307 (2014) 293–300.
[34] C. Fu, D. He, Y. Wang, X. Zhao, Synth. Met. 257 (2019) 116187.
[35] Z. Wang, J. Zou, Z. Ding, et al., Mater. Chem. Phys. 142 (2013) 119–123.
[36] G. Wang, L. Wang, Y. Gan, W. Lu, Appl. Surf. Sci. 276 (2013) 744–749.
[37] B. Zhao, J. Deng, L. Liang, et al., CrystEngComm 19 (2017) 6095–6106.